Fuel 248 (2019) 205–214

Contents lists available at ScienceDirect

Fuel

journal homepage: www.elsevier.com/locate/fuel

Full Length Article

Influence of carbon quantum dots on the viscosity reduction of polyacrylamide solution

Maje Alhaji Haruna[a], Zhongliang Hu[a], Hui Gao[a], Jabbar Gardy[a], Saminu Musa Magami[b], Dongsheng Wen[c,a,*]

[a] School of Chemical and Process Engineering, University of Leeds, Leeds LS2 9JT, England, UK
[b] 17 Whinchat Avenue, Newton-le-Willows, Merseyside, UK
[c] School of Aeronautic Science and Engineering, Beihang University, Beijing, China

GRAPHICAL ABSTRACT

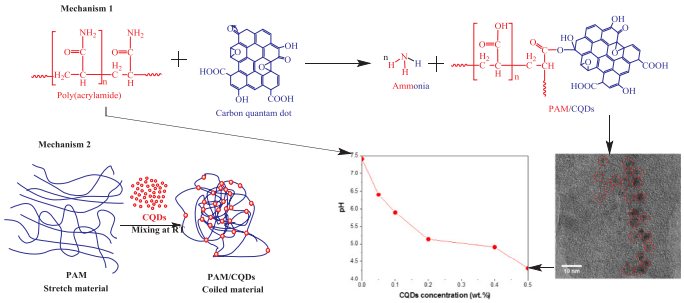

ARTICLE INFO

Keywords:
Rheology
Reduced viscosity
Polyacrylamide
Carbon quantum dots
Viscoelasticity

ABSTRACT

Viscosity is one of the key factors which influence the application of polyacrylamide (PAM) in enhanced oil recovery (EOR). In this study, we have demonstrated the viscosity reduction of PAM solution by using carbon quantum dots (CQDs) through rheological, spectroscopic and thermal analyses. The stability of PAM, CQDs, and PAM/CQDs composites, and the chemical interactions between PAM and CQDs were investigated. The addition of CQDs into PAM solution decreased its viscosity, demonstrating a phenomenon which contradicts the expression normally derived from the Einstein–Batchelor law for the viscosity of particle suspensions. Consequently, the elastic properties of PAM/CQDs composites were lower than those of the pure PAM solutions. Moreover, the presence of CQDs in the PAM increased its flow activation energy and decreased its yield point, leading to an increased sensitivity to both temperature and shear rate. The mechanism behind the reduced viscosity behaviour of PAM/CQDs composites appears to be the formation of free radicals and the elimination of ammonia molecules, leading to the deterioration of the polymer backbone.

1. Introduction

Recent studies have featured the structure-performance relationship in classical nanomaterials [1]. For example, fullerenes have been shown to intensify the performance of polymer-based photovoltaic appliances [2,3] and to help control the polymer's flow characteristics [4–6]. Some studies have shown that the inclusion of nanoparticles into polymer matrices could cause viscosity reduction [7–11], in a clear

* Corresponding author at: School of Chemical and Process Engineering, University of Leeds, Leeds LS2 9JT, UK and School of Aeronautic Science and Engineering, Beihang University, Beijing, 100191, PR China.
E-mail addresses: d.wen@leeds.ac.uk, d.wen@buaa.edu.cn (D. Wen).

https://doi.org/10.1016/j.fuel.2019.03.039
Received 21 November 2018; Received in revised form 25 February 2019; Accepted 6 March 2019

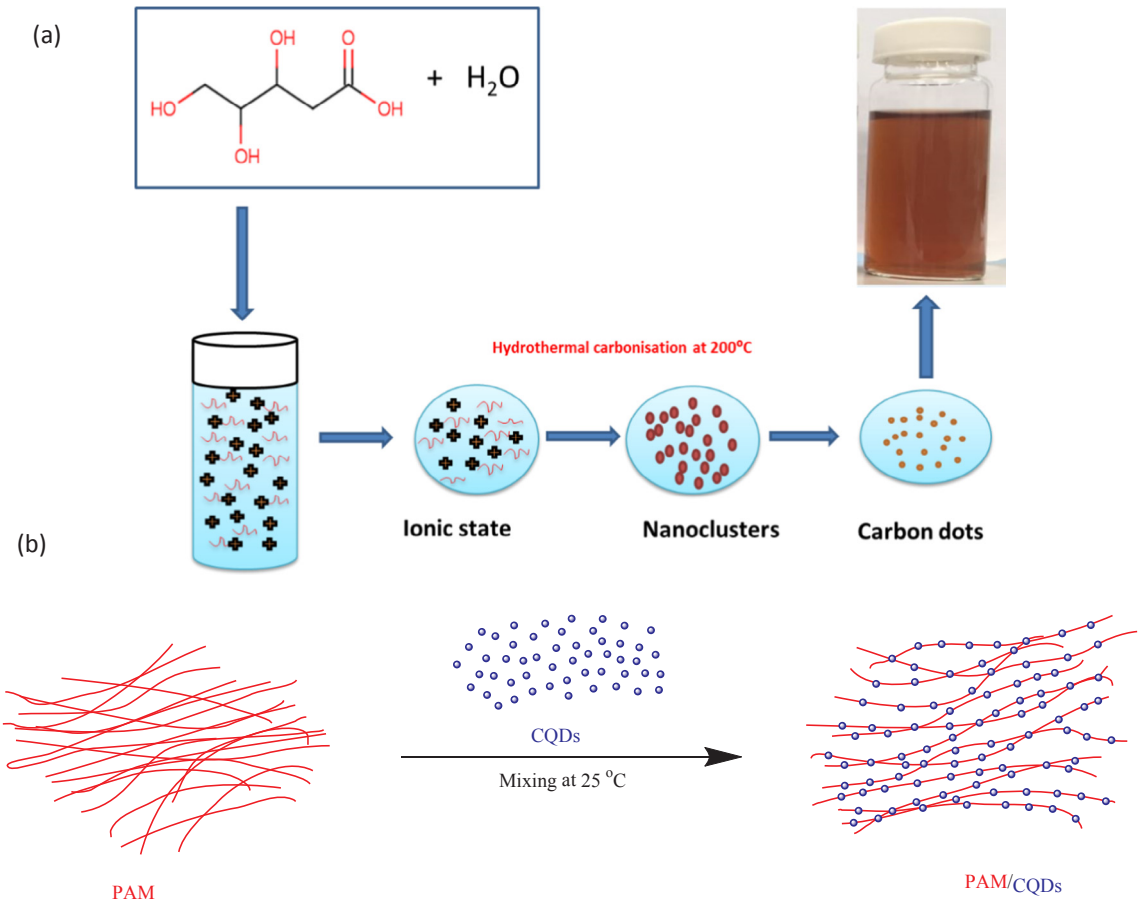

Scheme 1. Schematic of the synthesis of carbon quantum dots by one-step hydrothermal carbonisation of D-(+)-Xylose (a) and illustration of the synthesis of the PAM/CQDs composite materials (b).

disagreement to the expression developed by Einstein [12]. This phenomenon brings great attention with controversial explanations and perceptions [13–18]. It has been observed that the radius of nanoparticles, their radius of gyration and the molecular weight of the polymers are the leading factors affecting the behaviour of the polymer-nanoparticle composites [7–9]. According to studies by Mackay and coworkers [7–9], viscosity reduction occurred when the polymer molecular weight was larger than the entanglement molecular weight and the inter-particle half-gap was smaller than the gyration radius. Other studies show that degradation of the polymer [19,20], adsorption of polymers with high molecular weight [21], constraint release of the entangled polymer chain [8,9,18], free volume expansion induced around the nanoparticles [8,9], changes in the entanglement density of polymer chains [11] and slip between the sample and the geometry during rheological testing [4] are possible mechanisms that enable viscosity reduction in polymer–nanoparticle composites.

Recently, viscosity reduction arising from the addition of nanoparticles into polymers has been observed in linear and star-shaped polymers [7–11,22–24]. Polyacrylamide (PAM) is a water-soluble polymer that has been widely used for tertiary enhanced oil recovery, wastewater treatment, drag reduction, and drug delivery, and conformance control for improving sweeping efficiency [25–28]. It is usually known that the viscosity of PAM is usually determined by its molecular weight, chemical structure, degree of hydrolysis, polymer concentration, and affected by many environmental parameters [23]. Recent work has employed nanoparticles to improve the performance of PAM for different applications. For example, the combination of PAM with carbon quantum dots (CQDs) has been used for high resolution bio-imaging and drug delivery applications [29–32]. SiO_2 nanoparticles have been used to enhance the rheological properties of PAM for enhanced oil recovery applications [5]. There is, however, no study on the effect(s) of nanoparticle addition on the viscosity reduction of PAM. Contradictory to many other studies that the effective viscosity is generally increased with the addition of nanoparticles, our initial study suggested a different trend by applying CQDs into PAM. In this work, we report a comprehensive study of the effect of CQDs on the rheological behaviour of aqueous PAM solutions. Here CQDs were synthesized using one-step hydrothermal carbonisation of D-(+)-Xylose and used to examine the influence of the nanoparticles addition on the viscosity reduction of polyacrylamide solution. Such work could provide strong implications for different PAM based engineering applications to design suitable nanoparticles with engineered rheological behaviour of PAM

2. Materials and methods

2.1. Materials and synthesis of CQDs and PAM/CQDs

Water soluble PAM was purchased from Shandong Tongli Chemical Co. Ltd., China with molecular weight and relative density of 5–22 million g/mol and of 1.302 g/cm^3, respectively. CQDs were facilely synthesised by one-step hydrothermal carbonisation of D-(+)-Xylose, according to published procedures [33,34]. Firstly, 0.2 g of D-(+)-Xylose were dissolved in deionised water (20 ml). Afterwards, the solution was moved into a Teflon-lined, stainless steel autoclave. The solution was subsequently heated for 6 h at 200 °C and then cooled to room temperature. The cooled solution was centrifuged for 30 min at 10,000 rpm in order to obtain a solid black carbon precipitate. The supernatant containing carbon quantum dots was filtered using a standard syringe filter paper and then used in the next stage.

Composites of PAM/CQDs were prepared using mechanical mixing.

0.025 g of the PAM were dissolved in 50 ml deionised water to achieve 0.05 wt% PAM solution through continuously stirring at room temperature. Different concentrations (0.05, 0.1, 0.2, 0.4 and 0.5 wt%) of the CQDs were then separately added into the designated reactor containing PAM solution under gentle stirring at room temperature. Each PAM/CQDs suspension was gently stirred for 24 h to allow sufficient time for proper dispersion of the CQDs particles into the polymer matrix, as shown in Scheme 1(a) and (b). The CQDs particles and the PAM/CQDs composites were oven-dried in order to obtain powdered for further characterization. However, for SEM analysis a freeze-dried method was used to resulting in the powdered PAM/CQDs composites.

2.2. Characterisation techniques

Morphologies of the fabricated CQDs, PAM polymer and PAM/CQDs composites were determined by scanning electron microscopy (SEM, SU8230 Hitachi). The microscope was operated at 2 kV. Also, a transmission electron microscopy (TEM, FEI Tecnai TF20, LEMAS centre, Leeds, UK) was used, operated at 200 kV. The zeta potential was measured using a dynamic light scattering (DLS) technique (Zetasizer Nano ZS, Malvern Instruments Ltd., Malvern, UK). A UV–visible spectrometer (UV-1800, Shimadzu, Kyoto, Japan) was used to determine the particle concentrations, based on the Beers-lambert law. For this, measurements were carried out at the wavelength of 310 nm [35]. The stability of the PAM/CQDs composites was determined with a vertical scan analyser Turbiscan MA 2000 (Formulation, Toulouse, France) [36]. The functionality of the PAM, the CQDs, and the PAM/CQDs composites was measured by a Nicolet iS10 Attenuated Total Reflectance (ATR)-Fourier transform infrared (FTIR) spectrometer. The pH value of the composites was determined by a Mettler Toledo pH-meter (Seven Compact S210).

Thermal stability of the samples was studied using a TGA/DSC-1 instrument (Mettler Toledo, England), covering the temperature range of 35–900 °C. A heating rate of 10 °C/min was used during each measurement, the system was operated under constant flow rate of nitrogen gas at 50 ml/min. A TA Discovery Hybrid Rheometer (DHR-2, TA instruments) was used with a cone-and-plate geometry, for both shear and oscillatory rheological measurements. The measurement temperature was controlled by an advanced Peltier system which had a temperature accuracy of 0.1 °C. Each sample was measured three times to ascertain the repeatability and reproducibility of the results. For the purpose of obtaining flow kinetic data, shear measurements were conducted on the CQDs and on the CQDs/PAM at 25 °C and 85 °C, in addition to temperature sweep measurements that were carried out on the same materials. Proton NMR spectroscopy was carried out on the PAM and the PAM/CQDs composites, using advanced 600 MHz nuclear magnetic resonance spectrometer (Bruker Company, Ettlingen, Germany). Each specimen was tested in deuterium oxide (D_2O) solvent.

3. Results and discussion

3.1. Characteristics of the fabricated CQDs, PAM and PAM/CQDs composites

Fig. 1a shows images depicting the morphological characteristics of the PAM/CQDs composites. The TEM image, (Fig. 1a bottom right), reveals that the CQDs are spherical particles, having diameters in the region of ~5 nm. In this, no clear aggregations were observed. Thermal stability characteristics of the CQDs, the PAM and the PAM/CQDs composite material are presented in Fig. 1b. In the case of the CQDs, the thermogram indicates an initial weight loss (~13 wt%) after the commencement of the heating, until about 100 °C. This weight loss arises due to the evaporation of loosely held water molecules. Tightly held water was then steadily lost (~3 wt%) as the heating continued up to 150 °C. A steady decrease in weight (~66 wt%) was then observed until 600 °C, indicating the decomposition of the CQDs material. This decomposition is consistent with previous literature reports [37–40]. It can be seen that the PAM and the PAM/CQDs composite material showed a limited weight loss (~7 wt%), corresponding to the evaporation of loosely bound water molecules. This occurs through desorption of the molecules from the surface of the PAM and the PAM/CQDs composite at room temperature up until 150 °C. However, water molecules that are tightly bound to either the PAM or to the PAM/CQDs composites were desorbed between 150 and 230 °C. This result clearly indicates that water desorption occurred at a higher temperature in both PAM and PAM/CQDs materials in comparison to temperature it occurs in the CQDs particles. The decomposition curve corresponding to heating between 230 and 460 °C indicates the slow decomposition of the PAM molecules compared to the behaviour of the PAM/CQDs composite. This could be attributed to the amount of oxygen (as hydroxyl and carboxylic acid) reduction that occurs at elevated temperature in the PAM/CQDs material. It should also be noted that a significant weight loss in the PAM material was observed in the region of 460–900 °C. This can be attributed to release of ammonia molecules (deamination of PAM), accompanying the decomposition of formed carboxylic groups through pyrolysis at higher temperature. The thermal degradation and stability mechanisms of the PAM and PAM/CQDs are very complicated, which deserves further detailed studies by using differential scanning calorimetry (DSC), thermogravimetric analysis/mass spectrometry (TGA-MS) and/or thermogravimetric analysis-Fourier transform infrared (TGA-FTIR) techniques.

The static position method is the most generally used method to decide the stability of nanofluids. The static position method allows nanofluids to stand in a container for a particular period, and the distance or colour difference in sedimentation between nanofluids was observed by the naked eye [41–44]. In this study, the stability of nanofluids was determined using static and dynamic tests. The selected samples were evaluated via eye test investigation, turbiscan analysis, and zeta potential measurement. In the static position method, all samples remained standing for 10 days, and the stability difference between samples was observed by the naked eye. However, as shown in Fig. S1 (electronic supplementary information), the differences were difficult to detect using naked eye observation. The stability behaviour of the various materials was examined by the sedimentation method monitored every 1 h, continuously for 24 h, using a Turbiscan analyser (Fig. 2b). The technique detects changes in the backscattered light that are caused by the particle sedimentation within the sample cell. All of the samples with different CQD concentrations demonstrated no particle precipitation throughout the height of the container, indicating excellent stabilities. Fig. 2a shows that in comparison with the zeta potential of bare PAM, the zeta potential of the PAM/QCDs composite is much stronger, indicating that improved dispersion stabilization was achieved. For example, the zeta potential of the PAM/CQDs composite (0.4 wt% CQDs) reached up to ~ −55 mV due to the enhanced surface charges that were achieved through the addition of the PAM material.

ATR-FTIR spectroscopy was employed to analyse the behaviour of the chemical bonding between the PAM and the CQDs, as shown in Fig. 3a. In the spectrum of the CQDs, three peaks appear at 1117, 1449 and 2953 cm^{-1}. These peaks correspond to the vibration of C–O–C stretching, the methyl C–H bending and the C–H stretching, respectively. The peaks observed in the PAM spectrum at 3321 and 2923 cm^{-1} can be attributed to the hydroxyl (O–H) and the amino (N–H) groups in the PAM material. On the other hand, a broader peak has shifted to a lower wavenumber (3302 cm^{-1}). This could have arisen due to the formation of carboxylic acid in the backbone chains of the polymer in the PAM/CQDs composite. Moreover, a peak at 2953 cm^{-1} in the PAM/CQDs spectrum could be related to the C–H stretching vibration. New peaks also appeared in the spectrum of the PAM/CQDs at 1081 and 1451 cm^{-1}. These peaks are related to the formation of C–O stretching vibration and to methyl C–H bending vibration, respectively. This could be due to the existence/formation of ester cross-link bond between the PAM and the CQDs materials [5,45]. Additionally, the

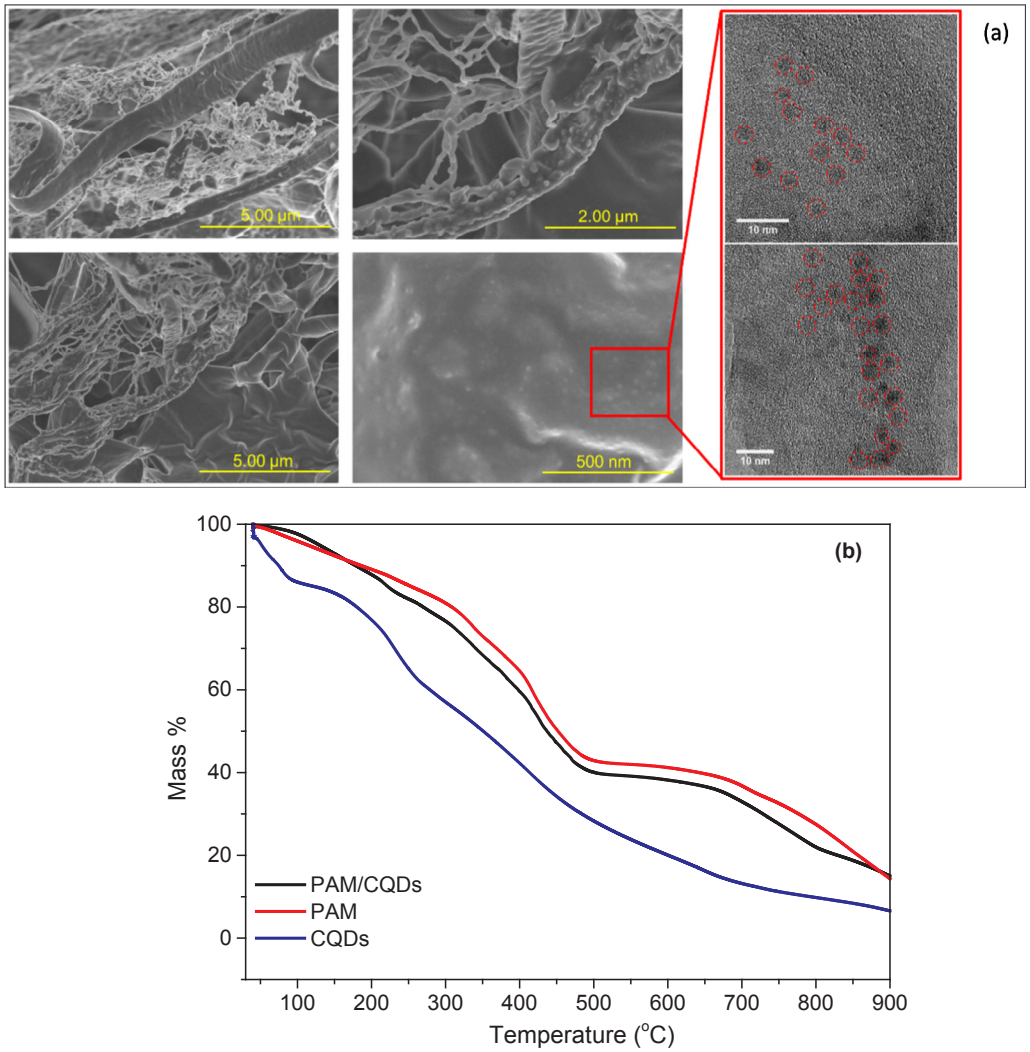

Fig. 1. (a) Morphological SEM (left) and TEM (right) images of the PAM/CQDs composite and (b) TGA profiles for CQDs, PAM, and PAM/CQDs composites.

absorption band formed at 1741 cm^{-1} is ascribed to carbonyl stretching vibration for the CQDs, as is the band at 1568 cm^{-1} which relates to –CO–O–C vibration stretching. There are other characteristic strong peaks between 1325 and 1386 cm^{-1}, representing the fingerprint region of C–O–C bonds and/or ester bonds (–CO–O–C). These peaks confirm the formation of a covalent bond between the carboxyl group in the deaminated polymer and the hydroxyl group in the CQDs.

Remarkably, the results from the ATR-FTIR analyses suggest the evolution of chemical ligation between the PAM segments and the CQDs in the composite material. With respect to a covalent bonding, the composites are observed and considered as stable enough to circumvent the possible phase separation that can easily happen in fabrication of the nanocomposites via physical mixing of polymer and carbon dots. The measured pH values (Fig. 3b) showed an increased acidity corresponding to an increase in the concentration of the CQDs. This is consistent with the release of $–NH_2$ molecules, forming NH_3. A more detailed explanation of this mechanism is discussed in Section 3.3.

The XRD profiles for the PAM and the PAM/CQDs composites are contained in Fig. S2, electronic supplementary information. In the case of the PAM/CQDs composite, two extra sharp diffraction peaks appeared at 2θ of 31.7 and 45.5°. These are related to the existence of small crystalline fractions of the PAM/CQDs composites. This clearly suggests that introducing the CQDs into the PAM transformed it from an amorphous status into a low degree of crystallinity. The NMR spectroscopy was used to evaluate the influence of the addition of the CQDs into the PAM. Fig. S3a and b, electronic supplementary information, show the proton NMR results of the PAM solutions and the PAM/CQDs composites, respectively. The peaks appear at 1.4 and 2.1 ppm represent protons in $–CH_2$. In the PAM material, $–CO–NH_2$ and C–H peaks were observed around 6.3 ppm and 6.9 ppm, respectively. These confirm the formation of major polyacrylamide functional groups in the spectrum [46–48]. However, the $–NH_2$ peaks in the PAM spectrum disappear in the PAM/CQDs composite, certainly proving the deamination from the polymer backbone by the presence of the CQDs.

3.2. Effect of CQD concentrations on viscosity reduction

Different CQDs concentrations were used to investigate the influence of the CQDs on the viscosity reduction of the PAM polymer. Both the PAM and the PAM/CQDs composites showed shear-thinning behaviours with an increase in shear rate, as shown in Fig. S4, electronic supplementary information. Fig. 4a shows 1000 s^{-1} shear viscosity as a function of the CQDs concentration for 25 and 85 °C, respectively. It can be clearly seen that with the addition of the CQDs, the effective viscosities decreased significantly at both temperatures. The higher the CQDs concentration, the lower was the effective viscosity. A nearly linear relationship in viscosity reduction was observed at 25 °C, corresponding to a change from 3.3 to 57.2% as the CQDs concentration was increased from 0.05 to 0.5 wt%. As expected, a much lower effective viscosity is found at 85 °C. However, the effect of the addition of the

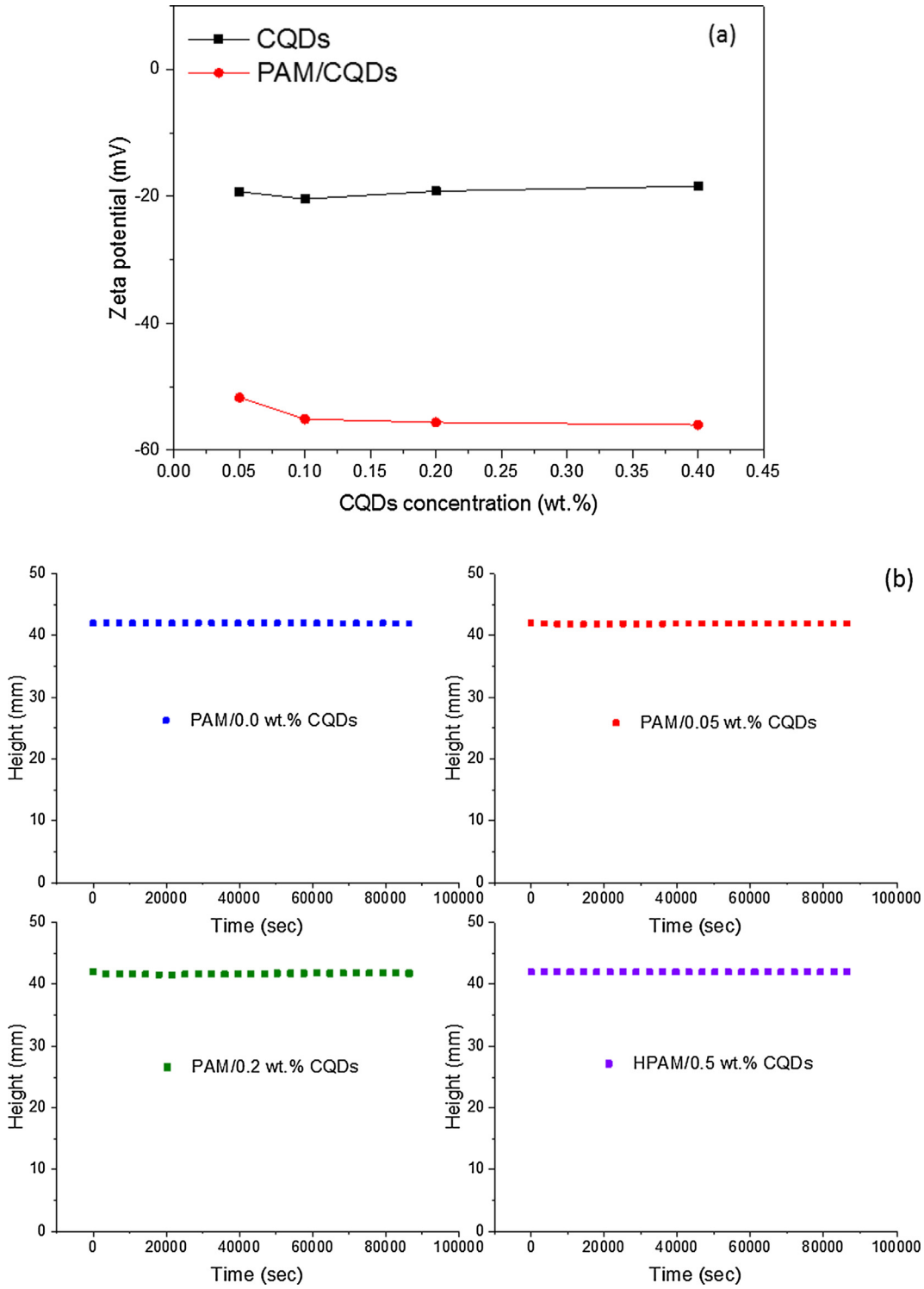

Fig. 2. (a) Zeta potential of PAM, CQDs and PAM/CQDs composites at different concentrations of the CQDs and (b) Turbiscan stabilisation tests after 24 h of PAM and PAM/CQDs composites containing different amount of CQDs.

CQDs is more pronounced, especially at the CQDs concentrations < 0.4 wt%. A sharp decrease of the effective viscosity by 27.7% was observed at 0.05 wt%, and the reduction continued, reaching 85.2% at 0.5 wt% loading of the CQDs. Similar viscosity reduction was reported by Yasufumi et al. for some PAM/silica nanoparticle suspensions. Such reduction was ascribed to the PAM adsorption on the surface of silica particles, resulting in the decrease in the amount of polymer in the mixture, and hence a reduction of the effective viscosity [49]. We found that such reduction is possible due to the dissociation of the PAM. This is discussed in detail in Section 3.3. In contrast, aqueous solutions of typical PAMs show Newtonian behaviour, with their effective viscosities slightly increasing with an increase in the concentration of CQDs. This is consistent with the conventional thought. It is expected that when the CQDs are dispersed in water, water molecules are likely bonded onto the surface of the particles due to its high polarity (hydroxyl O–H, carbonyl C═O and carboxylic –CO–OH groups), thereby causing the suspension viscosity to remain unchanged.

The effect of the addition of the CQDs on the viscoelastic properties

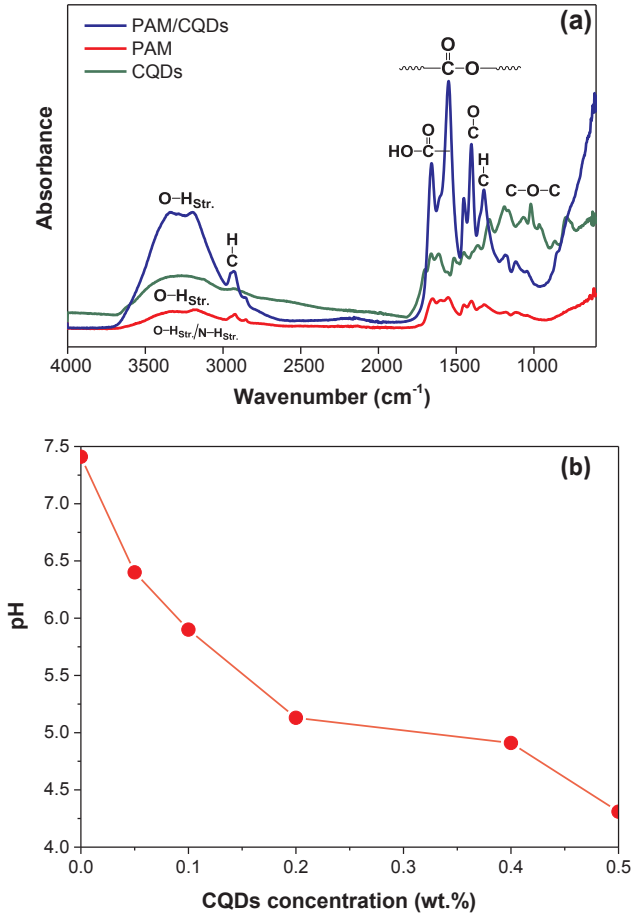

Fig. 3. (a) ATR-FTIR spectra and (b) monitoring of pH while addition of CQDs to the PAM solution was undertaken.

of the PAM was examined by a linear oscillatory frequency sweep test. The results obtained for the storage modulus (G′) and the loss modulus (G″) are plotted against angular frequency (ω) (Fig. 4b). The results showed a decrease in both G' and G'' with the addition of the CQDs into the composite. This indicates that the composite material becomes less elastically dominant.

As shown in Fig. S5, electronic supplementary information, the damping factor (tan δ) increases with the CQDs addition in the solution. Generally, a value of tan $\delta > 0.1$ accompanied by its comparatively small dependence on frequency is agreed to be the symptomatic character of a so-called weakened gel solution [50]. Here, it was observed that when the concentration of the CQDs was increased, the value of tan δ also increased. Therefore, it can be deduced that the addition of the CQDs into the PAM matrix formed elastically weaker material compared to the neat PAM. Furthermore, compared to the aqueous suspension of the PAM/CQDs material, pure PAM displayed less frequency dependence behaviour for both G' and G'', showing a good tendency of transition from liquid-like to solid-like viscoelastic state.

The complex viscosity $\mu^*$of the PAM and the PAM/CQDs composite obeys similar changing trends as observed for (G′) and (G″), as a function of (ω) (Fig. 5a). The complex viscosity (μ^*) of the PAM/CQDs composite (containing 0.05 wt% CQDs) was lower than that of the pure PAM. This could not be explained by the Einstein–Batchelor law for the viscosity of a particle suspension [4]. As the concentration of the CQDs in the composite was increased to 0.5 wt%, the μ^* continued to decrease. It was found that the value of $\mu^*$for the PAM/CQDs composite was lower than that of the pure PAM solution.

To support the above findings, the continuous relaxation spectra of the solutions was also calculated from the results of G′ and G″. The

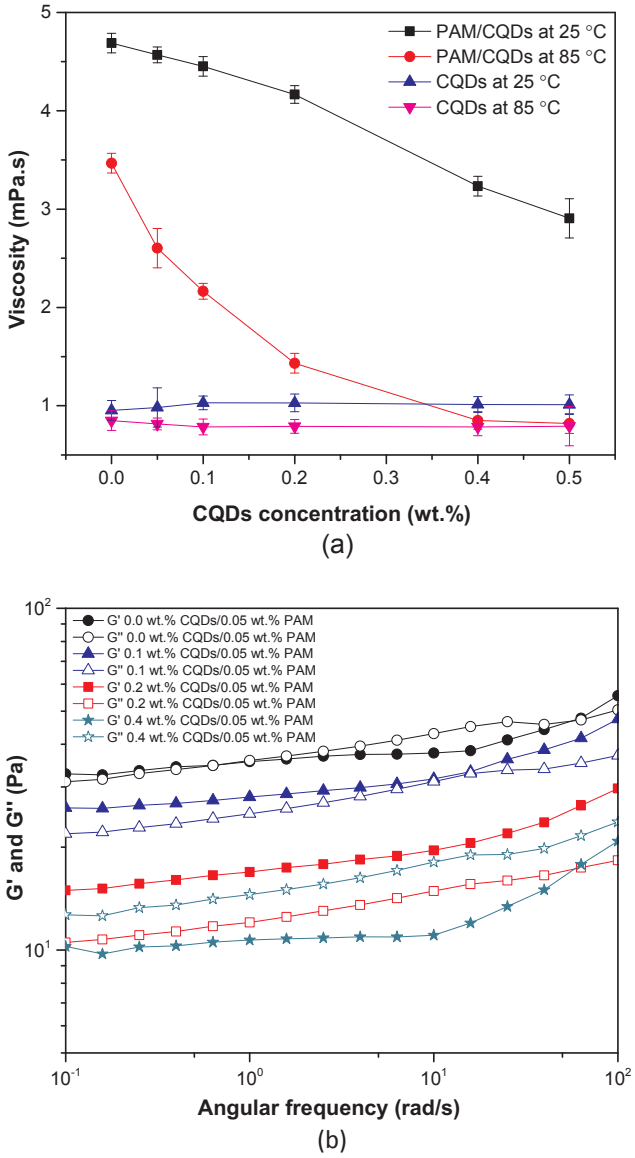

Fig. 4. (a) Viscosities of 0.05 wt% PAM with different concentrations of the CQDs, T = 85 and 25 °C, shear rate 1000 s^{-1}), (b) Storage modulus (G') and loss modulus (G").

TRIOS software available with the HDR-2 rheometer was used to calculate the continuous relaxation spectra, using the analysed G′ and G″data, respectively. The continuous relaxation time spectrum can be extracted by fitting the following model in terms of either oscillation [G′ (w), G″w)] or relaxation [G(t)] data. The theoretical basis for the relaxation expressions are given in Eqs. (1)–(4). Fig. 5b shows the continuous relaxation spectra of the PAM solution and that of the PAM/CQDs composite, as a function of the relaxation time. In comparison to the relaxation behaviour of the pure PAM solution, the relaxation time of the PAM/CQDs composite was shorter. The solutions containing higher concentrations of the CQDs (0.2 and 0.4 wt%) show a significant effect on the continuous relaxation spectrum of the PAM solution, especially at a short time scale. Therefore, it can be deduced that the PAM solution possesses long-term relaxation time as a result of sufficient links and associations between its macromolecules. This suggests that the mechanism behind the reduced viscosity behaviour of the PAM/CQDs composites is bounded by the relaxation effect of the samples.

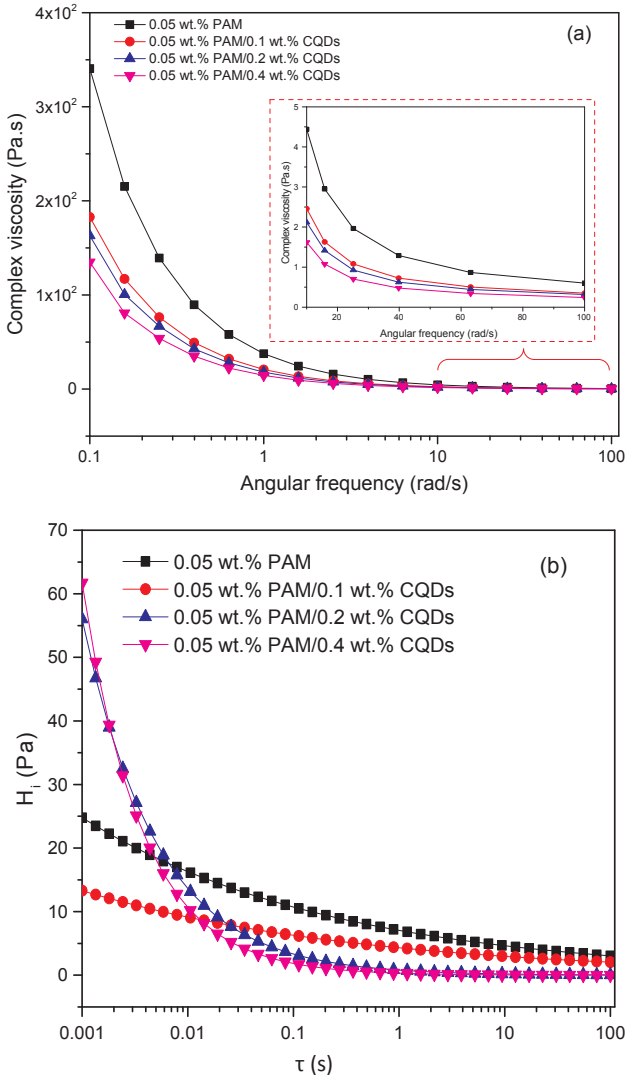

Fig. 5. (a) Complex viscosity for PAM and PAM/CQDs composites, with different concentrations of the CQDs, as a function of angular frequency (b) Continues relaxation spectra of PAM and PAM/CQDs composites, as a function of relaxation time.

$$dln\tau = \frac{d\tau}{\tau},\ g(\tau) = H(ln\tau) \tag{1}$$

$$G(t) = G_e + \int_{-\infty}^{+\infty} H(ln\tau)e^{-t/x}dln\tau \tag{2}$$

$$G' = \int_{-\infty}^{+\infty} H(ln\tau)\frac{\omega^2\tau^2}{1+\omega^2\tau^2}dln\tau \tag{3}$$

$$G'' = \int_{-\infty}^{+\infty} H(ln\tau)\frac{\omega\tau}{1+\omega^2\tau^2}dln\tau \tag{4}$$

In Eqs. (1) to (4), H is the continues relaxation spectrum, τ is the relaxation time and G(t) is the relaxation data.

$$k = Ae^{\frac{-Ea}{RT}} \tag{5}$$

$$\tau^{1/2} = \tau_0^{1/2} + \mu_\infty^{1/2}\gamma^{1/2} \tag{6}$$

In Eqs. (5) and (6), k is the rate constant, T is the absolute temperature, A is the pre-exponential factor, E_a is the flow activation energy, R is the universal gas constant, $\tau_0$is the yield stress, $\mu_\infty$is the suspension/solution viscosity at infinite shear rate, and $\dot{\gamma}$ is the shear rate.

The rheological results were given a kinetic treatment using the flow Arrhenius relationship (Eq. (5)) and the Casson-Asbeck equation (Eq. (6)) [51]. These relationships are widely applied to polymeric systems [52]. Thus, values were obtained for the yield point/stress (YP), the flow activation energy (FAE) and the infinite shear viscosity (ISV) for the CQDs, the PAM and the PAM/CQDs composite, as shown in Table 1. The plot of ln(viscosity) vs 1/T, used in modelling the flow kinetics of PAM, CQDs and PAM/CQDs is shown in Fig. S6, electronic supplementary information. Differences in the yield point, the infinite shear viscosity and the activation energy of flow can be seen. The yield stress is sensitive to the shear history, as the corresponding un-sheared materials have yield values more than the sheared ones. The lower value of yield stress obtained for the PAM/CQDs composite shows that the material has higher shear sensitivity in comparison to the corresponding PAM material. This effect arises as a result of the rapid movement and subsequent breakdown of structural linkages that priory exist between the CQDs and the PAM materials. According to Table 1, the PAM/CQDs composite has the highest value of flow activation energy of 745 kJ/mol compared to the pure PAM, indicating a high sensitivity to the influence of temperature during any potential applications.

Table 1
Data obtained from kinetic treatment of rheological plots, at 25 °C, on the basis of the flow Arrhenius equation and the Casson-Asbeck relationship.

Solutions	YP (Pa)	FAE (kJ/mol)	ISV (mPa s)
CQDs	9.7×10^{-3}	1100	0.47
PAM	0.59	733	3.4
PAM/CQDs	0.58	745	9.2

3.3. Potential mechanisms of the viscosity reduction for PAM/CQDs composites

Clearly the reduction of effective polymer viscosity by nanoparticle addition cannot be explained by conventional theories such as the Einstein-Batchelor relationship, which always states that the effective viscosity shall increase with an increase in particle concentrations. [53]. To account for this, two main mechanisms, including the free volume effect and particle agglomeration, have been proposed in the previous literature [10,11,18,54,55]. For the first mechanism, the viscosity reduction occurs in the polymer composites when the polymer was entangled and the nanoparticles were spherical [9]. Mackay et al. used a criteria of excluded free-volume around the nanoparticles to explain the decrease in the viscosity of nanoparticle-filled polymer melts [4]. They stated that the free volume was governed by the glass transition temperature (T_g) of the materials, and the increase of T_g indicated the reduction of the free volume [56]. As shown in Fig. 1b, based on our finding, the inclusion of the CQDs did not significantly result in the change of T_g of the PAM, and no direct relationship between the slight change in T_g and the reduction of viscosity of the PAM/CQDs composites was observed. Thus, the concept of increase in sample free volume, induced by the nanoparticles, cannot be considered as a plausible mechanism for the viscosity reduction of the PAM/CQDs composites.

For the second mechanism, it was reported that particle stability and aggregation could result in changes in the melt viscosity of polymer-nanocomposites during rheological measurements [57]. The results on the behaviour of PAM and PAM/CQDs composites from this study were analysed using a Turbiscan to investigate their stabilities (Fig. 3). The data showed no sedimentation for all the range of concentrations of the CQDs that were studied. Therefore, this excludes the influence of the aggregation of the CQDs and their stability as a possible reason for the observed viscosity reduction.

Clearly, the existing mechanisms cannot explain our current experimental results. It is proposed that the viscosity reduction is due to

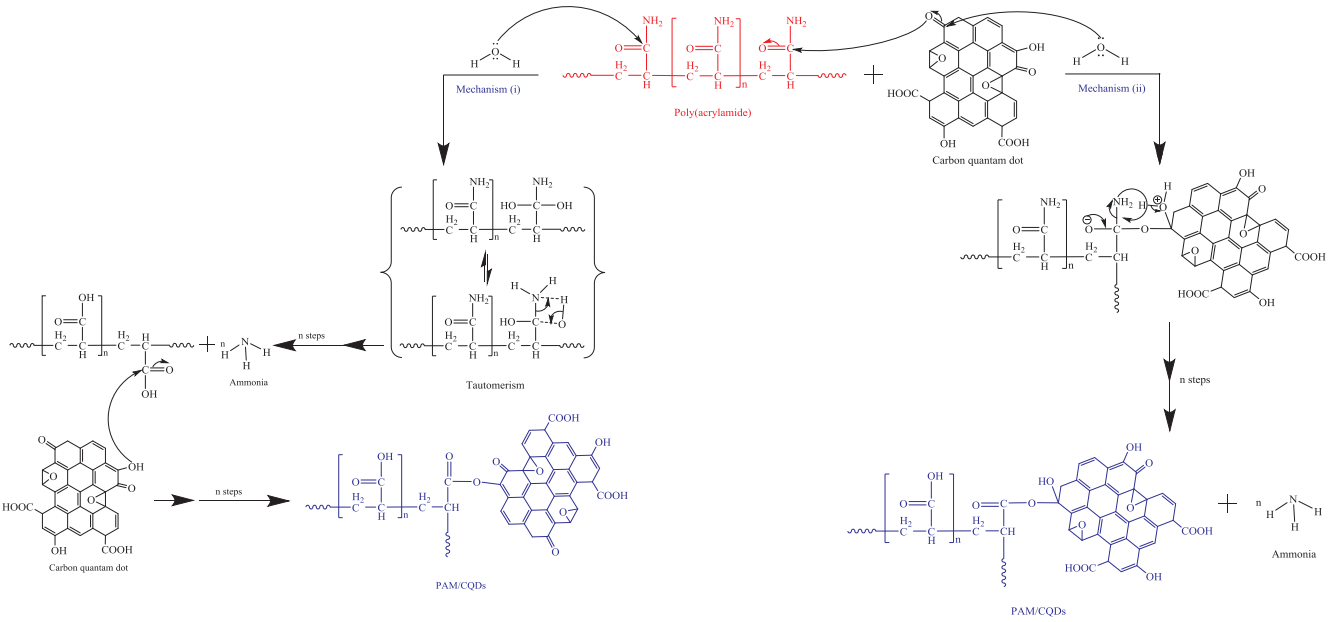

Scheme 2. Schematic illustration of proposed mechanistic pathways leading to the reduction of viscosity in the PAM/CQDs composites.

the degradation of PAM polymer by the deamination in the repeating unit of the polymer, leading to the formation of poly acrylic acid (PAA) and ammonia (NH_3) (Scheme 2). When the CQDs were included in the composites, the large number of oxygen containing groups in the CQDs attack the PAM material through nucleophilic reaction, thereby forcing it to release $–NH_2$ groups from the PAM repeating unit, leading to the formation of PAA and NH_3. These trends continue and deteriorate the polymer backbone, resulting in macromolecular degradation and the subsequent reduction of the PAM's ductility and embrittlement, hence the loss of viscosity. There are two proposed mechanistic pathways for the deamination and the formation of a covalent bond between the PAM and the CQDs materials, as shown in Scheme 2. In the case of the proposed mechanism (i), a nucleophilic attack on the carbonyl group in the CQDs is achieved via water molecules. This is then followed by nucleophilic addition of the CQDs onto the backbone of the PAM, leading to formation of unstable transition state. This then leads to the release of NH_3 molecules. However, according to mechanism (ii), the first step involves the elimination of NH_3 molecules from the PAM repeating unit before the addition of the CQDs.

Additionally, the CQDs could possibly make the PAM to transform from a stretch-state to a coil-state (Scheme 3). Since PAM is regarded as a polyelectrolyte, its viscosity and hydrodynamic size are responsive to the presence or addition of electrolytic functionalities. However, CQDs have been reported as cationic [58–60], and due to their electrolyte nature, when added to the PAM solution, they can cause protonation of the PAM's carboxylate groups into carboxyl groups ($–COO^-$ to –COOH). This then causes an increase in the acidity of the medium, being consistency with experimental result shown in Fig. 3b. This eventually causes a conformational transition of the polymer, changing from a stretch-conformation into a coiled-conformation (or shrinkable state). This then consequently leads to the reduction in the hydraulic radius and degree of entanglement of the polymer chain, eventually decreasing its viscosity.

4. Conclusions

The effects of the addition of CQDs into PAM solutions were investigated by the means of rheological, chemical and thermal analyses. The following outcomes can be drawn based on the results obtained:

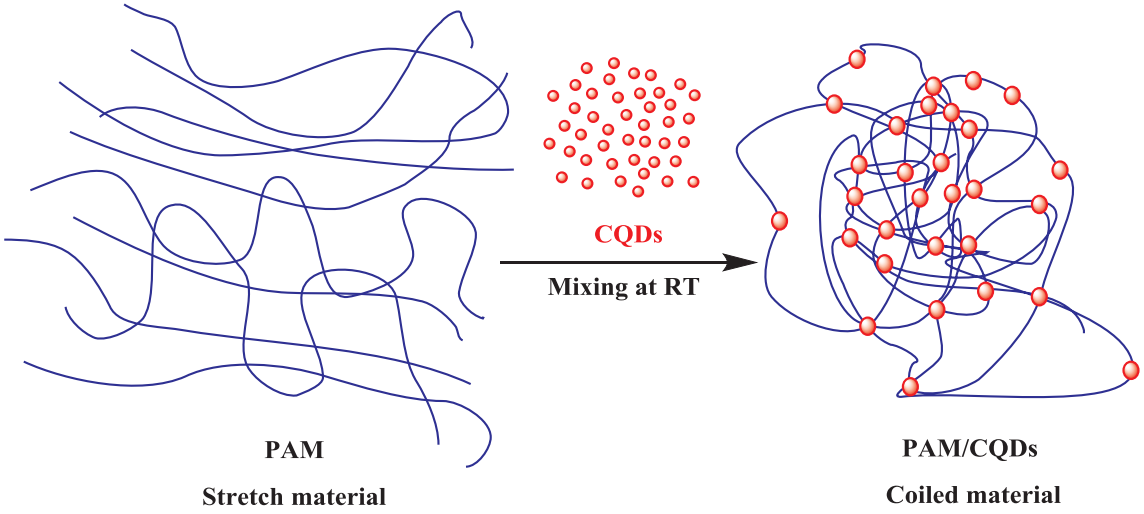

Scheme 3. Schematic showing how the PAM can change from a stretch-state into a coil-state.

The addition of CQDs decreases the viscosity of PAM suspensions. Both the storage and the loss moduli are decreased with an increase in the concentration of CQDs.

The ATR-FTIR analyses suggest the evolution of a chemical linkage between segments of PAM and those of CQDs. Thus, the formation of strong covalent bonding is achieved in the composite material between the deamination of the polymer backbone and the hydroxyl group in the CQDs.

The PAM/CQDs composite possesses a relatively higher value of flow activation energy of 745 kJ/mol, compared to the value exhibited by the pure PAM solution of 733 kJ/mol. This, indicates that the hybrid would be more sensitive to temperature, during any potential applications.

The results show that the mechanism behind the reduced viscosity behaviour of the PAM/CQDs composites arises from the relaxation effect of the samples, with the value of the relaxation parameter shorter in the PAM/CQDs composites, compared to that in the pure PAM.

Two possible schemes are proposed for the decreased viscosity phenomenon, which are: 1- formation of carboxylic acid groups on the PAM backbone, giving rise to a reaction with hydroxyl groups on the CQDs and the subsequent formation of ester bonds; 2- breakage of long macromolecular chains in the PAM into smaller chains, with the CQDs being able to protonate the carboxylate groups in the PAM ($–COO^-$ to –COOH), which make it more acidic and eventually cause a conformational transition of the polymer to change from a stretch-state into a coiled-state

Acknowledgments

The authors acknowledge the support of Petroleum Technology Development Funds (PTDF), Nigeria and the European Research Council (ERC-2014-CoG, Project reference: 648375).

Conflicts of interest

The authors declare no conflict of interest.

Appendix A. Supplementary data

Supplementary data to this article can be found online at https://doi.org/10.1016/j.fuel.2019.03.039.

References

[1] Camargo PHC, Satyanarayana KG, Wypych F. Nanocomposites: synthesis, structure, properties and new application opportunities. Mater Res 2009;12(1):1–39.
[2] Sariciftci NS, et al. Photoinduced electron transfer from a conducting polymer to buckminsterfullerene. Science 1992;258(5087):1474–6.
[3] Sariciftci N, Heeger A. Photophysics of semiconducting polymer-C60 composites: a comparative study. Synth Met 1995;70(1–3):1349–52.
[4] Mackay ME, et al. Nanoscale effects leading to non-Einstein-like decrease in viscosity. Nat Mater 2003;2(11):762.
[5] Hu Z, et al. Rheological properties of partially hydrolyzed polyacrylamide seeded by nanoparticles. Ind Eng Chem Res 2017;56(12):3456–63.
[6] Krishnamoorti R, Yurekli K. Rheology of polymer layered silicate nanocomposites. Curr Opin Colloid Interface Sci 2001;6(5–6):464–70.
[7] Mackay ME, et al. General strategies for nanoparticle dispersion. Science 2006;311(5768):1740–3.
[8] Tuteja A, et al. Effect of ideal, organic nanoparticles on the flow properties of linear polymers: non-Einstein-like behavior. Macromolecules 2005;38(19):8000–11.
[9] Tuteja A, Duxbury PM, Mackay ME. Multifunctional nanocomposites with reduced viscosity. Macromolecules 2007;40(26):9427–34.
[10] Schmidt RG, et al. A critical size ratio for viscosity reduction in poly (dimethylsiloxane) − polysilicate nanocomposites. Macromolecules 2010;43(23):10143–51.
[11] Gordon GV, et al. Impact of polymer molecular weight on the dynamics of poly (dimethylsiloxane)-Polysilicate Nanocomposites. Macromolecules 2010;43(23):10132–42.
[12] Einstein A. On the motion of small particles suspended in liquids at rest required by the molecular-kinetic theory of heat. Ann Phys 1905;17:549–60.
[13] Kropka JM, et al. Origin of dynamical properties in PMMA − C60 nanocomposites. Macromolecules 2007;40(15):5424–32.
[14] Mu M, et al. Polymer tracer diffusion exhibits a minimum in nanocomposites containing spherical nanoparticles. Macromolecules 2010;44(2):191–3.
[15] de Luzuriaga A. Key role of entropy in nanoparticle dispersion: polystyrene-nanoparticle/linear-polystyrene nanocomposites as a model system. PCCP 2008;10(5):650–1.
[16] Li Y, Kröger M, Liu WK. Nanoparticle effect on the dynamics of polymer chains and their entanglement network. Phys Rev Lett 2012;109(11):118001.
[17] Kalathi JT, Grest GS, Kumar SK. Universal viscosity behavior of polymer nanocomposites. Phys Rev Lett 2012;109(19):198301.
[18] Kim D, et al. Polymer nanocomposites: polymer and particle dynamics. Soft Matter 2012;8(42):10813–8.
[19] Cho J, Paul D. Nylon 6 nanocomposites by melt compounding. Polymer 2001;42(3):1083–94.
[20] Schulze D, et al. Rheological evidence of modifications of polypropylene by β-irradiation. Rheol Acta 2003;42(3):251–8.
[21] Jain S, et al. Strong decrease in viscosity of nanoparticle-filled polymer melts through selective adsorption. Soft Matter 2008;4(9):1848–54.
[22] Nusser K, et al. Viscosity decrease and reinforcement in polymer–silsesquioxane composites. Macromolecules 2011;44(19):7820–30.
[23] Tan H, et al. Melt viscosity behavior of C 60 containing star polystyrene composites. Soft Matter 2013;9(27):6282–90.
[24] Tan H, et al. Dependence of melt behavior of star polystyrene/POSS composites on the molecular weight of arm chains. J Phys Chem B 2014;118(19):5229–39.
[25] Haruna MA, et al. Improved polymer flooding in harsh environment by free-radical polymerization and the use of nanomaterials. Energy Fuels 2019.
[26] Green DW, Willhite GP. Enhanced oil recovery. In: Henry L, editor. Doherty Memorial Fund of AIME. Society of Petroleum Engineers; 1998.
[27] Haruna MA, et al. Improved rheology and high-temperature stability of hydrolyzed polyacrylamide using graphene oxide nanosheet. J Appl Polym Sci 2019:47582.
[28] Nourafkan E, et al. Improved rheological properties and stability of multiwalled carbon nanotubes/polymer in harsh environment. J Appl Polym Sci 2019;136(11):47205.
[29] Wang Y, Hu A. Carbon quantum dots: synthesis, properties and applications. J Mater Chem C 2014;2(34):6921–39.
[30] Bright CJ, et al. Quantum dot and polymer composite cross-reactive array for chemical vapor detection. Anal Chem 2015;87(24):12270–5.
[31] Tomczak N, Liu R, Vancso JG. Polymer-coated quantum dots. Nanoscale 2013;5(24):12018–32.
[32] Zhou Y, et al. Polymers in carbon dots: a review. Polymers 2017;9(2):67.
[33] Gao H, Wen D, Sukhorukov GB. Composite silica nanoparticle/polyelectrolyte microcapsules with reduced permeability and enhanced ultrasound sensitivity. J Mater Chem B 2015;3(9):1888–97.
[34] Gao H, et al. In situ synthesis of fluorescent carbon dots/polyelectrolyte nanocomposite microcapsules with reduced permeability and ultrasound sensitivity. ACS Nano 2016;10(10):9608–15.
[35] Shen C, et al. Kinetics of coupled primary-and secondary-minimum deposition of colloids under unfavorable chemical conditions. Environ Sci Technol 2007;41(20):6976–82.
[36] Hebishy E, et al. Physical and oxidative stability of whey protein oil-in-water emulsions produced by conventional and ultra high-pressure homogenization: Effects of pressure and protein concentration on emulsion characteristics. Innov Food Sci Emerg Technol 2015;32:79–90.
[37] Chen J, et al. Synthesis of silica-based carbon dot/nanocrystal hybrids toward white LEDs. J Mater Sci 2014;49(21):7391–8.
[38] Vázquez-Nakagawa M, et al. Chirality transfer from graphene quantum dots. Chem Commun 2016;52(4):665–8.
[39] Gaabour L. Spectroscopic and thermal analysis of polyacrylamide/chitosan (PAM/CS) blend loaded by gold nanoparticles. Results Phys 2017;7:2153–8.
[40] Al-Sabagh A, et al. Synthesis and characterization of high molecular weight hydrophobically modified polyacrylamide nanolatexes using novel nonionic polymerizable surfactants. Egypt J Pet 2013;22(4):531–8.
[41] Zhu D, et al. Dispersion behavior and thermal conductivity characteristics of Al2O 3–H2O nanofluids. Curr Appl Phys 2009;9(1):131–9.
[42] Phuoc TX, Massoudi M, Chen R-H. Viscosity and thermal conductivity of nanofluids containing multi-walled carbon nanotubes stabilized by chitosan. Int J Therm Sci 2011;50(1):12–8.
[43] Teng T-P, Lin L, Yu C-C. Preparation and characterization of carbon nanofluids by using a revised water-assisted synthesis method. J Nanomater 2013;2013:133.
[44] Li X, Zhu D, Wang X. Evaluation on dispersion behavior of the aqueous copper nano-suspensions. J Colloid Interface Sci 2007;310(2):456–63.
[45] Gao H, et al. Bifunctional ultraviolet/ultrasound responsive composite TiO 2/polyelectrolyte microcapsules. Nanoscale 2016;8(9):5170–80.
[46] Kavitha T, Abdi SIH, Park S-Y. pH-sensitive nanocargo based on smart polymer functionalized graphene oxide for site-specific drug delivery. PCCP 2013;15(14):5176–85.
[47] Kejun Y, Guowei Z. Synthesis and rheological properties in aqueous solution of poly (acrylamide-co-sodium allylsulfonate). J Appl Polym Sci 1992;44(1):1–7.
[48] Chen W, et al. Fabricating a flocculant with controllable cationic microblock structure: characterization and sludge conditioning behavior evaluation. Ind Eng Chem Res 2016;55(10):2892–902.
[49] Otsubo Y, Umeya K. Adsorption of polyacrylamide on silica particles and its effect on the rheological properties of suspensions. J Colloid Interface Sci 1983;95(1):279–82.
[50] Ikeda S, Nishinari K. "Weak Gel"-type rheological properties of aqueous dispersions of nonaggregated κ-carrageenan helices. J Agric Food Chem 2001;49(9):4436–41.
[51] Casson N. A new flow equation for pigment oile-suspension of the printing ink type.

Rheol Disperse Syst 1959.
[52] Magami SM, et al. The physical–chemical behaviour of amino cross-linkers and the effect of their chemistry on selected epoxy can coatings' hydrolysis to melamine and to formaldehyde into aqueous food simulants. Prog Org Coat 2015;78:325–33.
[53] Einstein A. Zur theorie der brownschen bewegung. Ann Phys 1906;324(2):371–81.
[54] Tuteja A, et al. Breakdown of the continuum stokes − Einstein relation for nanoparticle diffusion. Nano Lett 2007;7(5):1276–81.
[55] Kim SH, Ahn SH, Hirai T. Crystallization kinetics and nucleation activity of silica nanoparticle-filled poly (ethylene 2, 6-naphthalate). Polymer 2003;44(19):5625–34.
[56] Henckens A, et al. Synthesis of 3, 4-diphenyl-substituted poly (thienylene vinylene), low-band-gap polymers via the dithiocarbamate route. Macromolecules 2005;38(1):19–26.
[57] Des Cloizeaux J. Double reptation vs. simple reptation in polymer melts. EPL (Europhys Lett) 1988;5(5):437.
[58] Li H, et al. Water-soluble fluorescent carbon quantum dots and photocatalyst design. Angew Chem Int Ed 2010;49(26):4430–4.
[59] Yang W, et al. Cationic carbon dots for modification-free detection of hyaluronidase via an electrostatic-controlled ratiometric fluorescence assay. Anal Chem 2017;89(16):8384–90.
[60] Zhou J, et al. Cationic carbon quantum dots derived from alginate for gene delivery: one-step synthesis and cellular uptake. Acta Biomater 2016;42:209–19.